

<https://doi.org/10.1038/s42003-025-07703-x>

Common neuroanatomical differential factors underlying heterogeneous gray matter volume variations in five common psychiatric disorders



Shaoqiang Han^{1,2,3,4,5,6}  , Ya Tian^{1,2,3,4,5,6}, Ruiping Zheng^{1,2,3,4,5,6}, Qiuying Tao^{1,2,3,4,5,6}, Xueqin Song⁷, Hui-Rong Guo⁷, Baohong Wen^{1,2,3,4,5,6}, Liang Liu^{1,2,3,4,5,6}, Hao Liu^{1,2,3,4,5,6}, Jinmin Xiao⁸, Yarui Wei^{1,2,3,4,5,6}, Yajing Pang⁹, Huaifu Chen^{1,2,3,4,5,6,8} , Kangkang Xue^{1,2,3,4,5,6}  , Yuan Chen^{1,2,3,4,5,6}  , Jingliang Cheng^{1,2,3,4,5,6}   & Yong Zhang^{1,2,3,4,5,6}  

Multifaceted evidence has shown that psychiatric disorders share common neurobiological mechanisms. However, the tremendous inter-individual heterogeneity among patients with psychiatric disorders limits trans-diagnostic studies with case-control designs, aimed at identifying clinically promising neuroimaging biomarkers. This study aims to identify neuroanatomical differential factors (ND factors) underlying gray matter volume variations in five psychiatric disorders. We leverage 4 independent datasets of 878 patients diagnosed with psychiatric disorders and 585 healthy controls (HCs) to identify shared ND factors underlying individualized gray matter volume variations. Individualized gray matter volume variations are represented with the linear weighted sum of ND factors, and each case is assigned a unique factor composition, thus preserving interindividual variation. We identify four robust ND factors that can be generalized to unseen disorders. ND factors show significant association with group-level morphological abnormalities, reconciling individual- and group-level morphological abnormalities, and are characterized by dissociable cognitive processes, molecular signatures, and connectome-informed epicenters. Moreover, using factor compositions as features, we discover two robust transdiagnostic subtypes with opposite gray matter volume variations relative to HCs. In conclusion, we identify four reproducible and shared neuroanatomical factors that underlie the highly heterogeneous morphological abnormalities in psychiatric disorders.

Evidence from symptoms, as well as genetic and environmental risks, suggests that various psychiatric disorders share common neurobiological mechanisms^{1–3}. For example, vulnerability to psychiatric disorders thought to be driven by a general psychopathology dimension, Known as the “p factor”, which accounts for the positive correlations between symptoms⁴.

Genetic analyses have also identified common polymorphisms shared across multiple psychiatric disorders⁵. These findings support the idea that psychiatric disorders impact common neural circuits^{6,7}. In this context, neuroimaging studies and meta-analyses have sought to identify gray matter morphological differences shared by all disorders (transdiagnostic effects)^{8,9}.

¹Department of Magnetic Resonance Imaging, the First Affiliated Hospital of Zhengzhou University, Zhengzhou, China. ²Engineering Technology Research Center for detection and application of brain function of Henan Province, Zhengzhou, China. ³Engineering Research Center of medical imaging intelligent diagnosis and treatment of Henan Province, Zhengzhou, China. ⁴Key Laboratory of brain function and cognitive magnetic resonance imaging of Zhengzhou, Zhengzhou, China. ⁵Key Laboratory of Imaging Intelligence Research medicine of Henan Province, Zhengzhou, China. ⁶Henan Engineering Research Center of Brain Function Development and Application, Zhengzhou, China. ⁷Department of Psychiatry, the First Affiliated Hospital of Zhengzhou University, Zhengzhou, China. ⁸The Clinical Hospital of Chengdu Brain Science Institute, School of Life Science and Technology, University of Electronic Science and Technology of China, Chengdu, China. ⁹School of Electrical and Information Engineering, Zhengzhou University, Zhengzhou, 450001 Zhengzhou, China. ✉e-mail: shaoqianghan@163.com; xuekang08yx@163.com; chenyuanshizt@163.com; fccchengjl@zzu.edu.cn; zzuzhangyong2013@163.com

A recent meta-analysis by Goodkind et al. highlighted overlapping reductions in gray matter in the cingulate cortex and insula across psychiatric disorders¹⁰. However, challenges such as sample size, methodological standardization, and particularly the significant heterogeneity among patients with psychiatric disorders, limit the identification of clinically promising biomarkers.

Patients with psychiatric disorders demonstrate tremendous inter-individual variations in terms of symptoms, disease courses, therapeutic responses, and neuroimaging phenotypes^{11–14}. Neuroimaging studies have shown that group-level findings are only representative of only a handful of individual cases¹⁵. Despite the noticeable heterogeneity, previous neuroimaging studies relied almost exclusively on case-control approaches that focus on group-level effects, consequently leading to inconsistent or even conflicting findings¹⁶. In recent years, a growing number of researchers have begun to focus on individualized differences in neuroimaging measures via normative modeling^{15,17–19}. Similar to growth charts, normative modeling is used to construct normative expectations for biological measures of brain function (brain morphology, in most cases) based on demographic information of healthy cohorts. For a given patient, personalized differential patterns of the brain morphology are characterized by extreme deviations from the normal distribution¹⁷. By applying normative modeling to psychiatric disorders, researchers have quantified the neuroanatomical heterogeneity consistent with individual clinical manifestations and discovering potential psychiatric subtypes^{15,18–20}. Moreover, individualized deviations from normative range are strongly associated with treatment responses, suggesting its potential to guide the treatment of depression^{21,22}. These studies provide new insights into the etiology of psychiatric disorders and may facilitate precision medicine.

Although promising, previous studies on individualized morphological abnormalities have failed to explain the tremendous interindividual variations in the distributions of extreme deviations in patients with the same diagnosis. Deviation maps reveal notable heterogeneity among patients with psychiatric disorders, such as a regional extreme deviation is at most shared by 7% of individuals even with the same diagnosis^{8,15,18,19}. Heterogeneity contradicts the phenotypic similarities between cases with the same diagnosis. In a recent study, Segal et al. explain that phenotypic differences between cases are reflected in the heterogeneous localization of differential regions, whereas phenotypic similarities are in circuits/networks comprising of differential regions⁶. Here, we aimed to address this question from a dimensional perspective. Based on previous studies^{23,24}, we hypothesized that morphological differences in psychiatric disorders are commonly underlain by neuroanatomical differential factors (ND factors) reflecting phenotypic similarities, and that interindividual variability (phenotypic differences) is preserved by factor compositions.

This study aimed to identify ND factors underlying gray matter volume variations in five common psychiatric disorders: depression, schizophrenia, obsessive-compulsive disorder (OCD), bipolar disorder (BD) and attention-deficit/hyperactivity disorder (ADHD). We obtained individualized gray matter volume variations in each patient using normative modeling^{15,17–19} and identified ND factors across patients using non-negative matrix factorization (NMF)^{20,25}. As a data-driven multivariate method, NMF produces a sparse, parts-based representation of the data under non-negative constraints, producing more explanatory and reproducible results and avoiding the opposite differences canceling each other relative to other methods such as independent component analysis and principal component analysis²⁶. We hypothesized that person-specific morphological abnormalities could be represented as a linear weighted sum of ND factors, and each patient was assigned a unique factor composition, thus preserving interindividual variability. A series of sensitivity analyses were performed to assess the robustness and generalizability of the identified ND factors. To understand the ND factors, we investigated their relevance to group-level differences and cognitive processes. Furthermore, we showed that the identified ND factors were relevant to the distribution of neurotransmitter receptors/transporters and were informed by normal healthy connectome. Finally, we showed that factor composition aided the discovery of two neuroanatomical

subtypes with opposite gray matter volume variation differences relative to the healthy controls.

Results

Samples

This study included 4 independent datasets (1 discovery dataset and 3 validation datasets) of 878 patients with one of five psychiatric disorders and 585 healthy controls (HCs) from different ethnic groups. All analyses were conducted in the discovery dataset and validated in validation datasets, unless otherwise noted. The demographic and clinical information in the discovery dataset is presented in Supplementary Table S1. Sex, age and educational level did not significantly differ between the patients with HCs. Demographic and clinical information in the validation datasets is presented in Supplementary Table S2.

Four robust ND factors were identified

Consistent with a previous study²⁷, we parsed individualized gray matter volume variations into distinct differential patterns (ND factors) using non-negative matrix factorization (NMF) where individualized gray matter volume variations were measured as individual deviations (Z scores) derived from normative models^{15,17,27}. As there was no prior knowledge of the optimal number (K) of ND factors, we proposed a comprehensible metric, namely generalizability error (GE), to determine the optimal K, assuming that the optimal K would yield the most generalizable disease factors (See Methods). A higher GE indicated a worse generalizability. The GE reached minimum when the numbers of latent factors was two for both the positive and negative parts (Supplementary Fig. S1), suggesting that two positive and two negative ND factors are underlying morphological abnormalities in psychiatric disorders. For each factor, the most representative voxels (the top 10% of the voxels with the largest F values) are shown in Fig. 1 and Supplementary Table S3, and stratified into eight classical networks (seven cortical and one subcortical networks) as defined by Yeo et al.²⁸ (Fig. 1). Positive factor 1 mainly contained the bilateral temporal gyrus, postcentral gyrus, ventromedial prefrontal cortex/anterior cingulate cortex (vmPFC/ACC), and insula. Positive factor 2 mainly contained the bilateral striatum, vmPFC/ACC, bilateral thalamus, hippocampus, parahippocampal gyrus, amygdala and occipital lobe. Negative factor 1 mainly involved the vmPFC/ACC, bilateral hippocampus, superior frontal gyrus, bilateral insula, bilateral parahippocampal gyrus, middle cingulate cortex, and occipital lobes. Negative factor 2 mainly involved the bilateral middle and superior temporal gyrus. The spatial distributions of the ND factors and patient factor compositions are shown in Fig. 1, and the validation datasets are shown in Supplementary Figs. S4–S6.

We conducted a series of analyses to assess the reproducibility of the identified ND factors (see Methods). First, The 10-fold cross-validation (100 times) results showed that the identified ND factors predicted the factor compositions of unseen patients, with averaged Pearson's correlation coefficients between predicted factor compositions and true ones of 0.89 (± 0.01), 0.50 (± 0.04), 0.98 (± 0.00), and 0.87 (± 0.01) for positive factor 1, positive factor 2, negative factor 1, and negative factor 2, respectively. 2). Second, we applied trained NMF using patients with two disorders to predict the factor compositions of patients with the remaining disorder (leave-one-disorder-out cross-validation), to investigate the generalization of the identified ND factors to patients with unseen disorder. The leave-one-disorder-out cross-validation results showed that ND factors could significantly predict patients with unseen disorders. Specifically, for patients with depression, Pearson's correlation coefficients between the predicted factor compositions by models trained using patients with OCD and schizophrenia with true ones were $83.14e^{-2}$ for positive factor 1, $85.70e^{-2}$ for positive factor 2, $86.49e^{-2}$ for negative factor 1, and $87.20e^{-2}$ for negative factor 2. Likewise, for patients with OCD, Pearson's correlation coefficients were $99.95e^{-2}$ for positive factor 1, $99.65e^{-2}$ for positive factor 2, $99.94e^{-2}$ for negative factor 1 and $99.77e^{-2}$ for negative factor 2. For patients with schizophrenia, Pearson's correlation coefficients were $99.94e^{-2}$ for

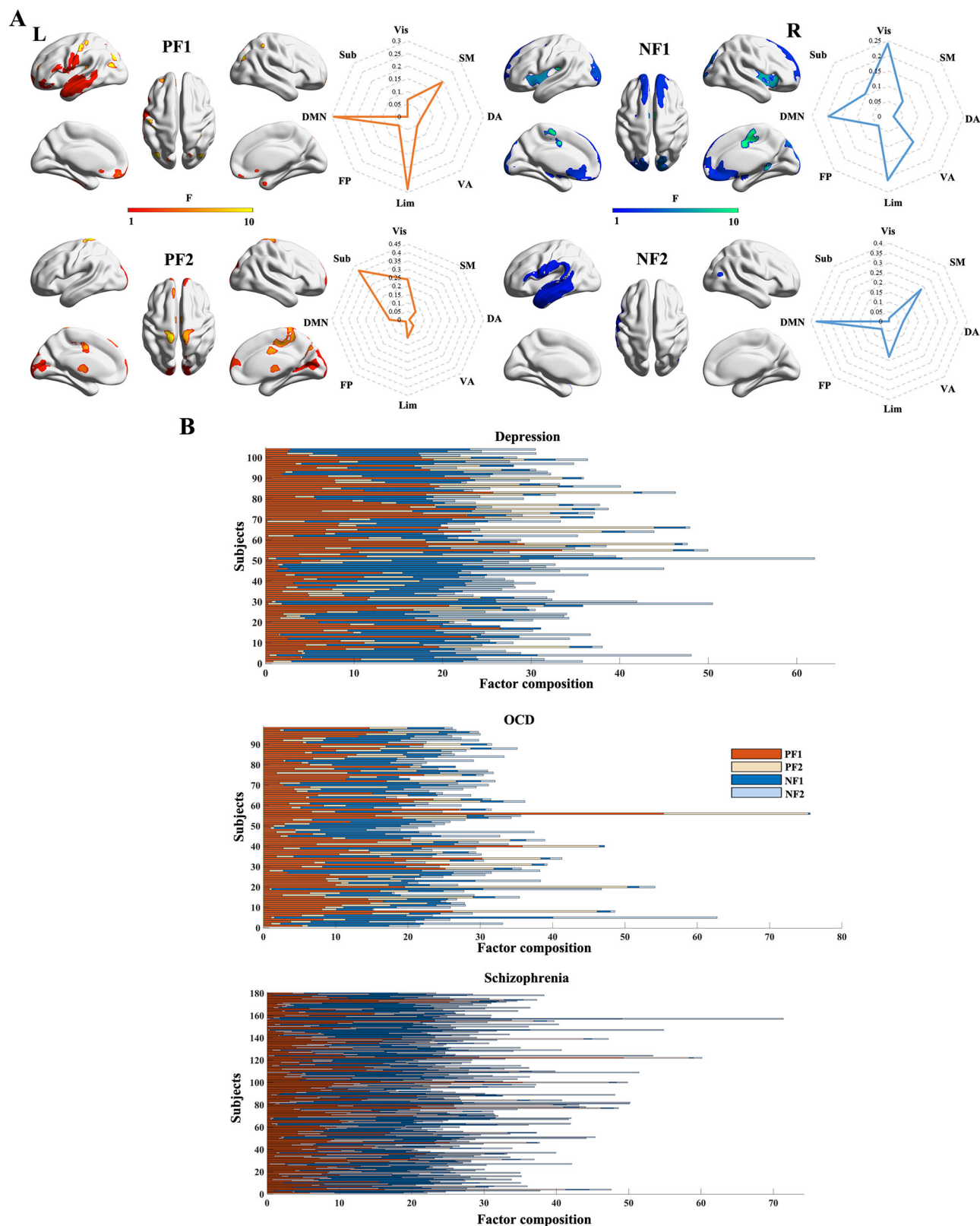


Fig. 1 | Spatial distributions of the identified ND factors and patient factor compositions (W). A Spatial distributions of the top 10% of the voxels with the highest F values for each factor and their overlap with classical networks. **B** Patient factor compositions. Note: PF1 positive factor 1, PF2 positive factor 2, NF1 negative

factor 1, NF2 negative factor 2, Vis visual network, VA ventral attention network, SM somatomotor network, Lim limbic network, DA dorsal attention network, FP frontoparietal network, Sub subcortical network, DMN default model network.

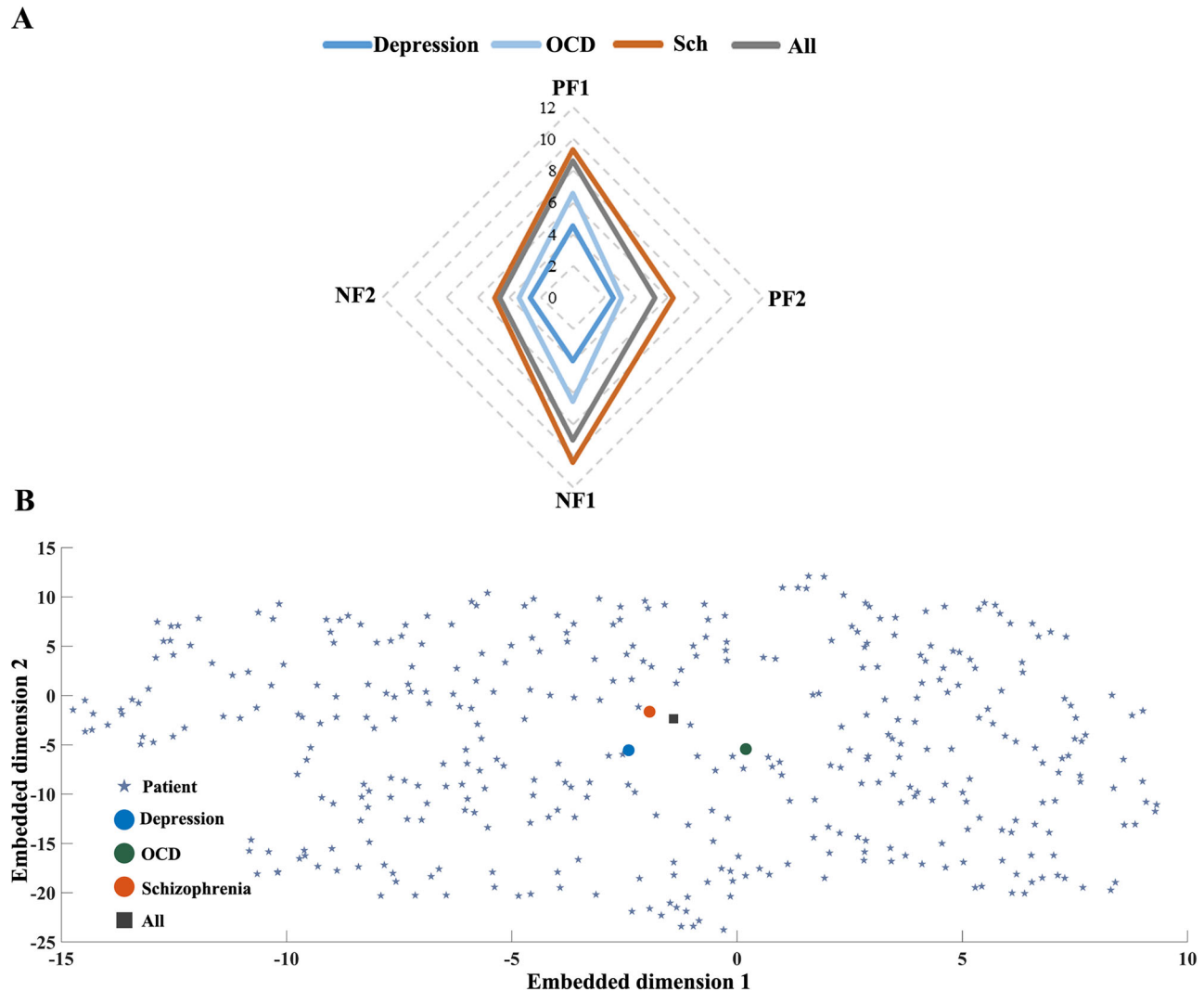


Fig. 2 | Association between ND factors and group-level morphological differences. **A** Estimated coefficients of multilinear models between group-level gray matter morphological differences (unthresholded T maps for patients vs. HCs) and ND factors for each disorder or all disorders. The numbers are the estimated

coefficients of multilinear models. The permutation $p < 0.001$ (FDR corrected).

B Factor composition of each patient and disorder (or all disorders) are embedded into two-dimensional space. Note: PF1 positive factor 1, PF2 positive factor 2, NF1 negative factor 1, NF2 negative factor 2.

positive factor 1, $99.66e^{-2}$ for positive factor 2, $99.83e^{-2}$ for negative factor 1, and $98.92e^{-2}$ for negative factor 2 (Supplementary Fig. S5 and Supplementary Table S7). All $p < 0.001$ (Benjamini-Hochberg false discovery rate (FDR) corrected). Third, the number of potential factors was consistently four (two positive and two negative factors) in the validation datasets (Supplementary Fig. S1). ND factors obtained using different datasets correlated significantly with each other with correlation coefficients of 0.21–0.57 (permutation testing $p < 0.001$, FDR corrected). Details are presented in Supplementary Fig. S6. Fourth, NMF trained using the validation dataset significantly predicted the factor compositions of patients in validation datasets. Specifically, Pearson's correlation coefficients between predicted factor compositions and true ones for positive and negative factors were 0.90 (95% CI = [0.84, 0.94]), 0.81 (95% CI = [0.70, 0.88]), 0.87 (95% CI = [0.79, 0.92]), and 0.54 (95% CI = [0.33, 0.70]) for validation set 1. 0.80 (95% CI = [0.75, 0.83]), 0.91 (95% CI = [0.89, 0.93]), 0.84 (95% CI = [0.80, 0.87]), 0.90 (95% CI = [0.87, 0.92]) for validation 2; and 0.79 (95% CI = [0.71, 0.85]), 0.65 (95% CI = [0.53, 0.74]), 0.88 (95% CI = [0.83, 0.92]), 0.57 (95% CI = [0.43, 0.68]) for validation set 3 (Supplementary Fig. S7). All FDR corrected $p < 0.001$. These results suggest that ND factors can be reproduced in independent datasets with different data acquisition equipment and

protocols, preprocessing strategies, medicine status, and races and can be generalized to unseen disorders.

Association between ND factors and group-level results

After confirming the robustness of the identified ND factors, we investigated whether ND factors could explain the traditional group-level morphological differences. To this end, we fitted a multilinear model of the group-level results (unthresholded T-maps for patients vs. HCs) and the ND factors for each disorder and all disorders. Group-level results were significantly derived from the ND factors for each disorder and all disorders. Specifically, the model goodness-of-fit (adjusted R^2) for depression, OCD, schizophrenia, and all disorders were 0.15 (F-statistic = $1.43e^4$), 0.40 (F-statistic = $5.47e^4$), 0.57 (F-statistic = $1.10e^5$), and 0.76 (F-statistic = $2.64e^5$), respectively. All FDR-corrected permutation $p < 0.001$. The estimated coefficients of the models are drawn in Fig. 2A. This association was similarly observed in the validation datasets (Supplementary Results).

To show, we embedded the factor composition of each disorder (estimated coefficients of multilinear models) and patient into a two-dimensional space (Fig. 2B) using a dimensionality reduction technique²⁹. This result confirmed that group-level results essentially represented an “average patient” for each disorder (or all disorders).

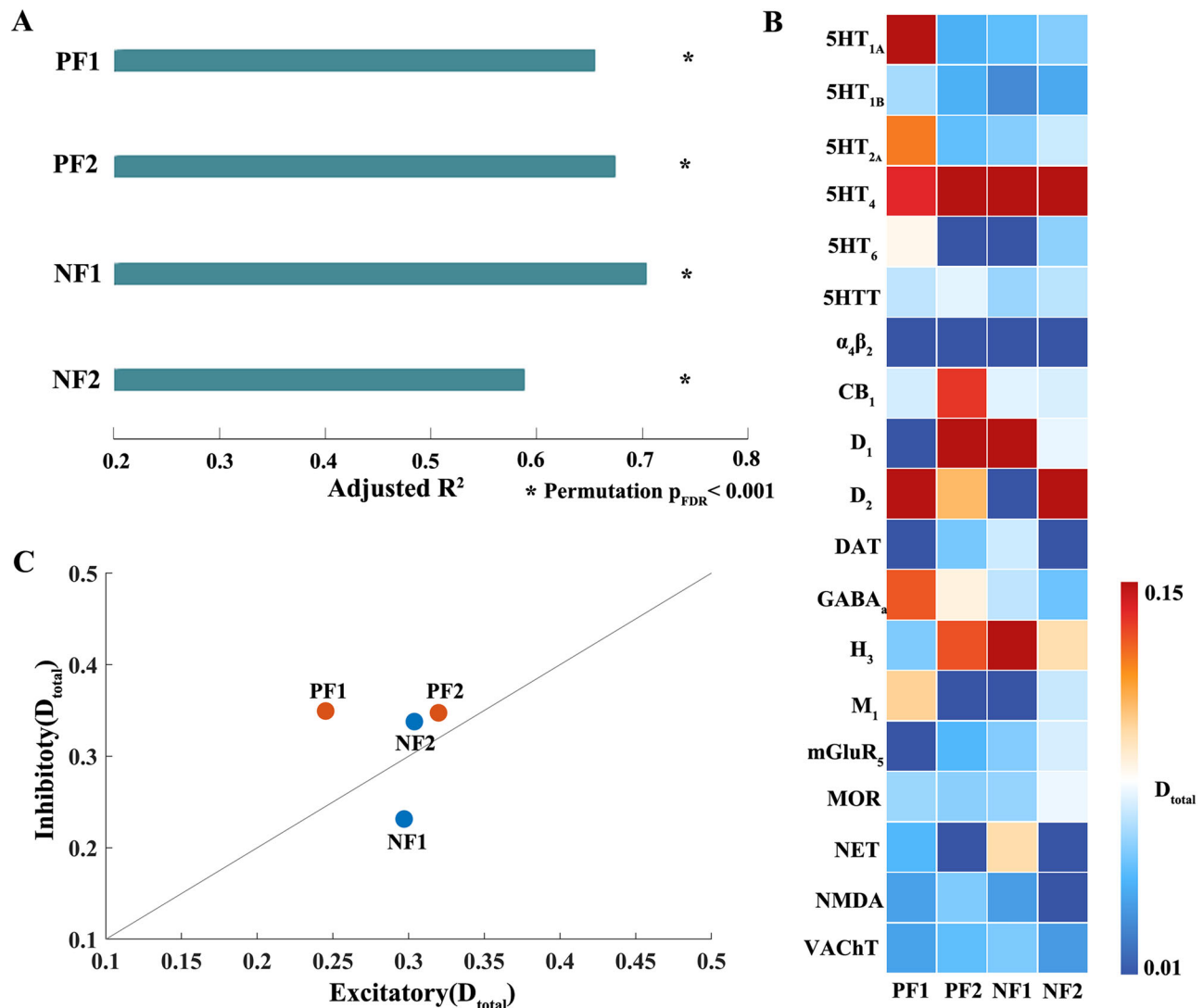


Fig. 3 | Contributions of neurotransmitter receptors/transporters to ND factors. **A** We construct four separate multilinear models of neurotransmitter receptors/transporters and each ND factor. The corresponding model goodness-of-fit (adjusted R^2) is shown in the bar plot. **B** Dominance analysis was performed for each multilinear model to determine the relative importance of the predictors. The total dominance values, measuring the relative importance of the predictors, are shown.

C We stratified receptors into excitatory and inhibitory receptors and calculated their accumulated contributions (by summing the total dominance values) to the ND factors. The accumulated contribution of excitatory receptors (Excitatory_ D_{total}) was plotted against that of inhibitory receptors (Inhibitory_ D_{total}). The gray line indicates the identity line. Note: PF1 positive factor 1, PF2 positive factor 2, NF1 negative factor 1, NF2 negative factor 2.

Association between ND factors and dissociable cognitive domains

To investigate the relationship between ND factors and cognitive processes, we performed functional annotation for each factor. Functional annotation showed that the identified ND factors corresponded with distinct cognitive domains (uncorrected permutation $p < 0.05$; Supplementary Fig. S8). Most of these terms did not survive the FDR correction. We used this tolerant threshold because the representative brain areas of the ND factors are primarily located in association cortices that are implicated in diverse but not specific cognitive processes. Broadly, positive factor 1 was associated with multisensory integration, and positive factor 2 was associated with attention deficits and emotions. In contrast, negative factor 1 was implicated in attention and executive functions, whereas negative factor 2 was implicated in auditory and social functions. Additionally, we validated this association at different top n% (8% and 12%) of the voxels for each factor and the results remain largely unchanged (Supplementary Figs. S9–S10).

Association between neurotransmitter receptors/transporters and ND factors

Psychiatric pathology can be informed by local molecular attributes, such as neurotransmitter receptor profiles³⁰. Therefore, we investigated the contribution of molecular vulnerability to the identified ND factors. To this end, we fitted four multilinear models of neurotransmitter receptors/transporters and each ND factor separately. The significance of the multilinear models was assessed using one-sided permutation testing (10000 permutations) and corrected for multiple testing with FDR correction. For each positive and negative factors, the model goodness-of-fit (adjusted R^2) were 0.56 ($F(68,48) = 5.44$, FDR-corrected permutation $p < 0.001$), 0.72 ($F(68,48) = 10.2$, FDR-corrected permutation $p < 0.001$), 0.68 ($F(68,48) = 8.53$, FDR-corrected permutation $p < 0.001$) and 0.65 ($F(68,48) = 7.66$, FDR-corrected permutation $p < 0.001$) (Fig. 3A).

A dominance analysis was conducted for each multilinear model to determine the relative importance of the predictors (neurotransmitter receptors/transporters). The dominance analysis showed that: 5HT₄ is

consistently important for both the positive and negative factors. D_1 is important for positive factor 2 and negative factor 1, whereas D_2 is important for positive factor 2 and negative factor 2. Moreover, $5HT_{1A}$ and H_3 specifically contributed to positive factor 1 and negative factor 1, respectively. The total dominance values which indicate the relative importance of each predictor, are shown in Fig. 3B.

Moreover, we stratified the receptors into excitatory and inhibitory receptors and calculated their accumulated contributions (by summing the total dominance values) to the ND factors. We found that inhibitory receptors predominantly contributed to positive factor 1, whereas excitatory receptors predominantly contributed to negative factor 1. Excitatory and inhibitory receptors contributed comparably to positive factor 2 and negative factor 2 (Fig. 3C).

ND factors are anchored to dissociable disease epicenters

Recent neuroimaging studies have proposed that neuropsychiatric disorders target intrinsic brain networks. Pathological perturbations, measured with structural abnormalities, begin in focal brain regions ('epicenters') and propagate to other brain regions following normal brain network architecture^{31–34}. Raj et al. proposed a model named network diffusion model (NDM) to quantitatively test this progress³⁵. In NDM, the trans-neuronal transmission of pathology along axonal projections is considered as a diffusion process in the normal brain network, with gray matter volume variations serving as a measure of pathology³⁵. NDM has successfully captured the trans-neuronal propagation of pathology and even predicted the future longitudinal progression of pathology in neurodegenerative diseases^{35,36}. Moreover, NDM reveals the temporal sequencing of pathological progression, correctly recapitulating the Braak staging of Lewy pathology in Parkinson's disease³⁷. Based on these studies, we investigated whether the identified ND factors were informed by the normal structural covariance network.

The NDM outcomes (correlation matrices) for each factor are shown in Fig. 4A. As shown, when the NDM was seeded at the anterior cingulate cortex (ACC), right middle temporal gyrus, right precentral gyrus, and right putamen, the best recapturing of ND factors profiles was achieved (maximum correlation coefficients was obtained), suggesting that the regions were plausible seed regions (disease epicenters). Spatial correlation coefficients between NDM-predicted morphological abnormalities and ND factors were 0.29 (FDR corrected permutation $p < 0.001$), 0.14 (FDR corrected permutation $p = 0.040$), 0.30 (FDR corrected permutation $p < 0.001$), and 0.17 (FDR corrected permutation $p = 0.023$) for positive and negative factors (Fig. 4B).

Factor composition reveals two robust subtypes with opposite morphological abnormalities

Using factor compositions as features, K-means revealed two transdiagnostic subtypes (silhouette values are plotted in Fig. 5A). The average patient factor composition for each subtype is shown in Fig. 5B. There were 195 (51.05%) and 187 (48.95%) patients in subtype 1 and 2, respectively. The disorder composition of each subtype is shown in Fig. 5. These two subtypes did not significantly differ in terms of sex, age, symptom severity, illness duration, or age of onset (uncorrected $p > 0.05$) for each diagnosis. However, they demonstrated opposite morphological abnormalities compared with that of HCs (Bonferroni-corrected $p < 0.05$). Subtype 1 demonstrated GMV, mainly in the middle temporal gyrus, vmPFC/ACC, inferior frontal gyrus, middle frontal gyrus, insula, putamen, and precuneus. In contrast, subtype 2 showed a widespread decrease in GMV in almost all brain regions (Fig. 5). When mixed, the patients demonstrated no significant gray matter volume variations compared with the HCs (Bonferroni-corrected $p < 0.05$).

Sensitivity analysis revealed that the subtyping results using randomly selected subsamples were consistent with the main results, with the mean ARI reaching 0.84 (± 0.17). The ARIs are shown in Supplementary Fig. S11. We obtained subtyping results using another completely different algorithm (heterogeneity through discriminative analysis, HYDRA), with regional

GMV as features. The HYDRA showed that the optimal number of subtypes was 2 (Supplementary Fig. S12). In addition, the ARI between the HYDRA subtyping and the main results was 0.58. These results confirmed the robustness and reproducibility of the subtyping results.

Discussion

In this study, we identified four robust ND factors accounting for the heterogeneous morphological abnormalities in psychiatric disorders. The identified ND factors were reproducible using independent datasets and could be generalized to unseen disorders. The significant and quantified relationship between ND factors with group-level morphological abnormalities reconciled the individualized and group-level results. Furthermore, ND factors are characterized by dissociable cognitive processes, molecular signatures, and connectome-informed disease epicenters, suggesting distinct underpinnings. Moreover, factor composition revealed two robust transdiagnostic neuroanatomical subtypes, providing new insights into taxonomy of psychiatric disorders.

The identified ND factors exhibit robustness and reconcile morphological abnormalities at the individual and group levels. Although the identified ND factors were obtained from first-episode and untreated patients, they showed good reproducibility when validated using validation datasets with different data acquisition equipment and protocols, pre-processing strategies, medicine status and race. Further sensitivity analyses suggest that ND factors significantly predict factor compositions of unseen patients, and even patients with unseen psychiatric disorders. These results confirm the generalizability of the identified ND factors and indicate that they are shared by psychiatric disorders, reflecting transdiagnostic effects. Of note, ND factors also share brain regions. For instance, in charging multiple affective and cognitive functions, the ventromedial prefrontal cortex/anterior cingulate cortex belongs to both positive and negative factors. Neuroimaging studies have frequently reported structural abnormalities in this region³⁸. However, the findings have been inconsistent. For instance, both increased³⁹ and decreased³⁸ GMV have been reported in schizophrenia. This discrepancy can be explained by the existent of opposite differential factors underlying gray matter volume variations identified in this study. The overlapping brain regions of positive and negative factors suggest they have multifarious roles in the neurobiology of psychiatric disorders and provide a potential interpretation for conflicting findings in neuroimaging studies with case-control designs. Although they share common ND factors, patients with psychiatric disorders exhibit notable interindividual variations in factor compositions consistent with the notion that psychiatric disorders are highly heterogeneous^{11,13,40–43}. High heterogeneity reflects phenotypic differences among patients with psychiatric disorders. Moreover, the identified ND factors could significantly derive the observed group-level gray matter volume variations for each diagnosis (or all diagnoses), reconciling morphological abnormalities at the individual and group levels. Besides, the factor compositions of psychiatric disorders might reflect degree of abnormalities of psychiatric disorders, with schizophrenia > OCD > depression. This trend has been documented in previous studies^{44,45}. Unlike previous findings that highlighted regional overlaps as shared effects between disorders^{46–48}, this quantitative relationship between ND factors and group-level gray matter volume variations highlight how common neurobiology underlies seemingly irrelevant morphological abnormalities in different disorders. Individualized deviations in structural and functional brain measurements show promise for subject-level classification, identifying disease subtypes, and predicting prognosis^{49–51}. In the present study, the identified ND factors reveal two transdiagnostic subtypes with distinct patterns of structural abnormalities. Additionally, previous research has demonstrated that individualized deviations in gray matter morphology are strongly associated with treatment efficacy in patients with depression^{21,22}. Building on these findings, we hypothesize that ND factors may also hold promise for prognostic prediction, an area that warrants further investigation.

Receptor distribution contributes to cortical morphology in psychiatric disorders. Neurotransmitter dysfunction is thought to underlie psychiatric

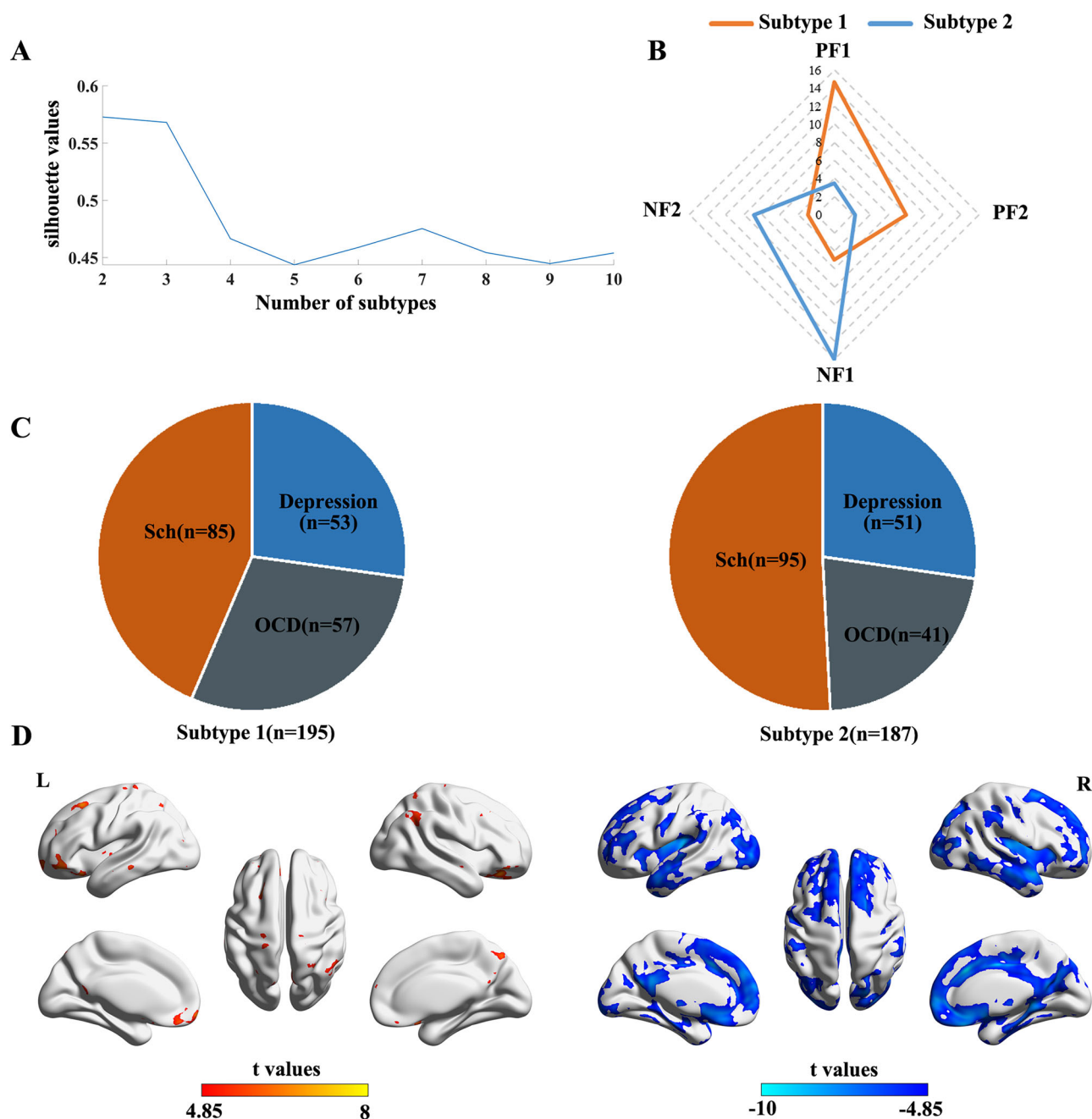


Fig. 4 | NDM performance. **A** Evolutional correlation matrices (R-t curves) between predicted and actual ND factors by sequentially seeding NDM at each brain region. Red lines indicate evolutionary correlations between the most plausible seed regions, whereas gray lines indicate those of non-seed regions. **B** Permutation testing results. Orange lines indicate the true performance (True R^2) of NDM on the actual network,

and the performance distribution (Permutation R^2) of NDM on random networks. **C** Disorder composition for each subtype. **D** Voxel-wise gray matter morphological differences of each patient subtype compared with that of the HCs (Bonferroni-corrected $p < 0.05$).

disorders, such as serotonin reuptake in depression and dopamine release in schizophrenia³⁰. Neurotransmitter receptor profiles are hypothesized to have close relationship with disorder-specific cortical abnormalities and cross-disorder similarities in brain disorders^{30,52}. The effectiveness of modern antipsychotic and antidepressant drugs depends on the selective manipulation of neurotransmitter function. In this study, neurotransmitter receptor/transporter distribution account for up to 72% of the variations observed in the identified ND factors, suggesting the fundamental contributions of neurotransmitters to ND factors. In addition, we show that some receptors (e.g. 5HT₄) are consistently important for positive and negative factors, whereas others are selectively important for some factors. Furthermore, we showed the dissociable associations between ND factors

and excitatory and inhibitory receptors profiles. Collectively, these results demonstrate the molecular signatures of the identified ND factors and provide potential clues for pharmacotherapy.

Moreover, the identified ND factors are significantly recapitulated by NDM seeding at distinct disease epicenters. In neuropsychiatric disorders, emerging evidences suggest that progression of pathology manifested as structural abnormalities, is constrained by or even forecasted by the normal network architecture^{34,53,54}. For instance, neuroimaging studies have shown that pathological perturbations begin at focal epicenters and propagate to unaffected brain regions^{31,32,54,55}. Consistent with the findings of these studies, we observed that the identified ND factors were significantly recapitulated by NDM, supporting the network-based spreading process model.

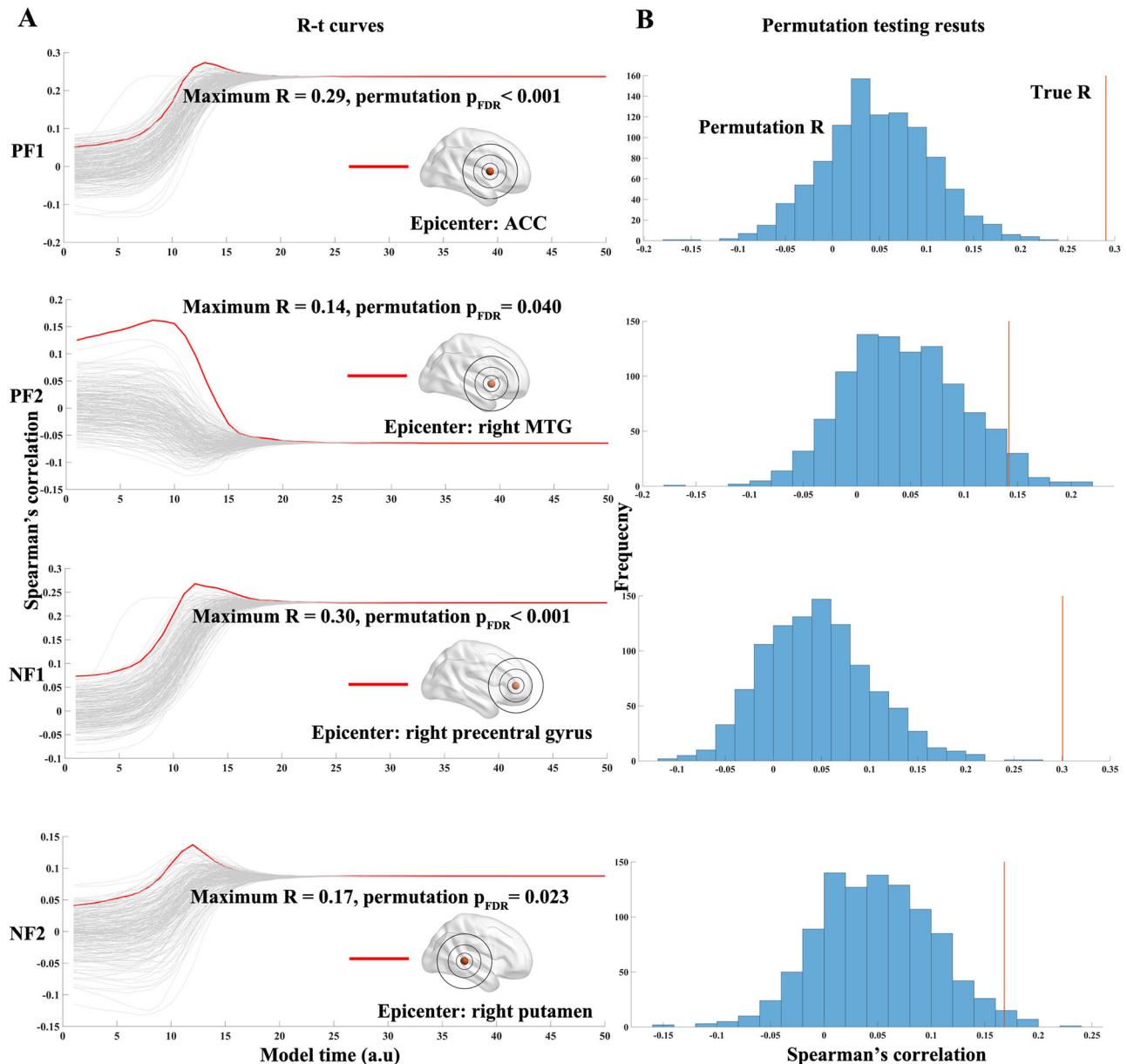


Fig. 5 | Subtyping patients into transdiagnostic subtypes based on factor compositions. A Silhouette values for each number of subtypes. B Averaged patients factor composition in each subtype.

The identified ND factors are associated with distinct disease epicenters that are located in the brain regions implicated in high-order cognitive/emotional and sensory/motor processes, possibly mirroring top-down and bottom-up dysregulation in psychiatric disorders^{56–60}.

Identification of more homogeneous psychiatric subtypes is expected to improve the understanding of etiological mechanisms⁶¹. Previous studies have identified subtypes based mainly on clinical manifestation^{62–64}. Despite great success, clinical manifestations have a complex interplay with the underlying biological substrates and are unstable with age or illness course. Identifying psychiatric subtypes from objective neuroanatomical data using data-driven approaches has gained increased popularity⁶¹. In this study, using factor compositions as features, we discovered two distinct neuroanatomical psychiatric subtypes. Sensitivity analysis confirms reproducibility of the subtyping results. Despite the notable morphological abnormalities, these two subtypes demonstrate similar clinical phenotypes. Notably, when combined, the patients show no significant differences compared with the HCs. Similar subtypes have been reported in schizophrenia, depression, and OCD separately^{39,65,66}. Taken together, these results

suggest that the identified ND factors aid the discovery of two robust transdiagnostic psychiatric subtypes, indicating the prospect of ND factors in clinical applications.

This study has some limitations. First, we did not have sufficient clinical information, such as medicine types and doses, and symptom dimensions (e.g. obsessive dimensions). Thus, we failed to investigate whether and how medicine modulated ND factors and whether ND factors corresponded to specific symptom dimensions. Second, for the discovery dataset, we only recruited patients without comorbidities with other psychiatric disorders, who often had more severe symptoms. Although the identified ND factors showed good consistency between patients with and without comorbidities, the effect of comorbidities on the factor compositions should be investigated in the future. Third, we only considered five psychiatric disorders, future studies should investigate whether ND factors can be generalized to more disorders. Fourth, although the identified ND factors obtained using untreated psychiatric patients can be reproduced in patients on medication, the specific effects of medication on our findings warrant further investigation in the future. Fifth, the current study did not

take symptom severity into account and we did not find significant associations between factor compositions and symptom severity (if any). Since the ND factors are shared across psychiatric disorders, they could be associated with common features not available in our study. These associations warrant further investigation. Finally, the neurotransmitter receptor profiles were obtained based on PET images of other samples. Future studies should verify the association between ND factors with neurotransmitter receptor profiles in the same samples.

In conclusion, we identify a reproducible and shared ND factors underlying gray matter volume variations in patients with psychiatric disorders, reflecting the phenotypic similarities across psychiatric disorders. With these factors, individualized gray matter volume variations can be represented as a unique and linear weighted sum of ND factors, reflecting the phenotypic differences between patients. ND factors are characterized by dissociable cognitive processes, molecular substrates, and connectome-informed disease epicenters and aid the discovery of two transdiagnostic subtypes with opposite differences compared with HCs. These results provide novel insights into the neuropathology of psychiatric disorders.

Methods

Overall approach

This study was organized as follows. We leveraged a discovery dataset of untreated and first-episode patients to identify shared ND factors from a dimensional perspective. The robustness and generalizability of the identified ND factors were assessed using independent validation datasets with different data acquisition equipment and protocols, preprocessing strategies, medicine status, and race. We investigated the relationship between ND factors and group-level gray matter volume variations. To interpret ND factors, we characterized them using distinct neurocognitive terms, neurotransmitter receptor/transporter distributions, and disease epicenters. Finally, using the factor compositions as features, we identified two subtypes with opposite gray matter volume variations relative to the normal population.

Datasets

Four independent datasets (1 discovery dataset and 3 validation datasets) of 878 patients and 585 healthy controls (HCs) with 5 psychiatric disorders from different ethnic groups were included in this study. The discovery dataset comprised the data of 383 patients with psychiatric disorders, including patients with depression ($n = 104$), schizophrenia ($n = 180$), OCD ($n = 98$), and matched healthy controls ($n = 130$). Validation dataset 1 was obtained from the Centre for Biomedical Research Excellence (COBRE) and is available at http://fcon_1000.projects.nitrc.org/indi/retro/cobre.html⁶⁷. The COBRE group comprised 72 patients with schizophrenia and matched 74 HCs. Validation dataset 2 was obtained from the Depression Imaging Research Consortium (DIRECT)^{68,69}. We used only the single-site dataset with the largest sample size (site 20) to prevent multi-site effects on our results. This dataset comprised the data of 282 patients with depression and matched 251 HCs. Validation dataset 3 was obtained from the University of California, Los Angeles (UCLA) Consortium and is available in the public database OpenfMRI⁷⁰. The dataset included the data of 142 patients with psychiatric disorders (schizophrenia, $n = 50$; ADHD, $n = 43$; BD, $n = 49$) and 130 HCs.

All study procedures were in accordance with the Declaration of Helsinki of 1975, and approved by the local Research Ethics Committees. All ethical regulations relevant to human research participants were followed.

Discovery dataset

This study was approved by the Research Ethics Committee of the First Affiliated Hospital of Zhengzhou University. Data of 382 patients (depression, $n = 104$; OCD, $n = 98$; schizophrenia, $n = 180$) and 130 healthy controls (HCs) were collected from the discovery dataset from the Department of Psychiatry of, the First Affiliated Hospital of Zhengzhou University, Zhengzhou, China. All study procedures were performed in

accordance with the Helsinki Declaration of Helsinki of 1975. All participants provided signed informed consent before the experiment.

Diagnosis was made by a chief physician and a well-trained psychiatrist based on the Diagnostic and Statistical Manual of Mental Disorders, Fourth Edition criteria. All patients were first episode and untreated and had no comorbidity with psychotic disorders, nervous system diseases/cardiovascular diseases, history of trauma or brain surgery, history of substance abuse, or medication use in the past month. Symptom severity of the patients with psychiatric disorders (depression, OCD, or schizophrenia) was assessed using the 17-item Hamilton Depression Scale (HAMD)⁷¹, Positive and Negative Symptom Scale (PANSS)⁷² and Yale–Brown Obsessive Compulsive Scale (Y-BOCS)⁷³, respectively. One hundred and thirty HCs were recruited from the adjacent community through poster advertisements. None of the HCs had a history of serious medical or neuropsychiatric illness and no family history of major psychiatric or neurological illness in their first-degree relatives.

Validation dataset 1

Validation dataset 1 was obtained from the center for biomedical research excellence (COBRE), available at http://fcon_1000.projects.nitrc.org/indi/retro/cobre.html⁶⁷. The COBRE consisted of 61 patients with schizophrenia and matched 73 HCs after excluding participants with poor image quality or missing data. Patients were diagnosed with schizophrenia according to the Diagnostic and Statistical Manual of Mental Disorders (DSM-IV, Fourth Edition). Patients were taking antipsychotic medications, and no medication changes within 1 month. The exclusion criteria included active substance dependence or abuse (except for nicotine) within the past 1 year and a history of neurological disorders. HCs were interviewed using the DSM-IV Axis I disorders-non-patient edition. None of the HCs had a history of depression or antidepressant use within the last six months, a history of lifetime antidepressant uses for more than one year, a recent history of substance abuse or dependence, head trauma with a loss of consciousness of >5 min, or a family history of psychotic disorder in a first-degree relative.

Validation dataset 2

Validation dataset 2 was obtained from site 20 of the Depression Imaging Research Consortium (DIRECT)^{68,69}, comprising the data of 282 patients with depression and 251 HCs. The patients were recruited from the First Affiliated Hospital of Chongqing Medical School, Chongqing, China. Two psychiatrists independently assessed the diagnoses according to the Structured Clinical Interview for DSM-IV. Patients had no comorbidity with other psychiatric disorders. Symptom severity was assessed using the HAMD⁷¹. HCs did not meet DSM-IV criteria for any psychiatric disorders nor have used any drugs that affect brain structure or function. All participants (both patients and HCs) meet the following exclusion criteria: current neurological disorders; a history of substance abuse; and serious encephalopathy. The procedures of this dataset were approved by the Research Ethics Committee of the Brain Imaging Center of Southwest University and the First Affiliated Hospital of Chongqing Medical School. All the participants provided signed informed consent.

Validation dataset 3

Validation dataset 3 was obtained from the University of California, Los Angeles (UCLA) Consortium for Neuropsychiatric Phenomics (CNP), which is available in the public database OpenfMRI⁷⁰. The dataset includes 142 patients with psychiatric disorders (schizophrenia, $n = 50$; BD, $n = 49$; ADHD, $n = 43$) and 130 HCs. This study was approved by the Institutional Review Boards at UCLA and the Los Angeles County Department of Mental Health, and all participants signed informed consent before the experiment. Diagnoses were made according to the Structured Clinical Interview for DSM-IV-Text Revision⁷⁰. The inclusion criteria for all participants include years of formal education of >8 years, absence of significant medical illness, and negative urinalysis results for drugs of abuse (e.g. Cocaine and Morphine). HCs had no lifetime diagnoses of psychotic/mental disorders, or Substance Abuse. Further details regarding the dataset are provided

elsewhere⁷⁰. Participants whose behavioral scores/images were missing or who had signal dropouts in the cerebellum were excluded⁷⁴. Finally, 224 participants were included, as described by Kebets et al.⁷⁴. Additional details are provided elsewhere^{70,74}.

Data acquisition

Discovery dataset. T1-weighted anatomical images were acquired on 3-Tesla GE Discovery MR750 scanner (General Electric, Fairfield Connecticut, USA) with the following parameters: repetition time = 8164 ms, echo time = 3.18 ms, flip angle = 7 degrees, voxel size = $1 \times 1 \times 1 \text{ mm}^3$, inversion time = 900 ms, thickness = 1.0 mm, resolution matrix = 256×256 , slices = 188.

Validation dataset 1

T1-weighted anatomical images of COBRE were acquired using Siemens Trio scanner. Scanning parameters were as follow: repetition time = 2530 ms, echo time = 1.64 ms, flip angle = 7 degrees, voxel size = $1 \times 1 \times 1 \text{ mm}^3$, inversion time = 1200 ms, field of view = 256 mm, resolution matrix = 256×256 , thickness = 1.0 mm, 256 slices.

Validation dataset 2

T1-weighted anatomical images were scanned on a 3.0-T Siemens Trio MRI scanner using a 16-channel whole-brain coil (Siemens Medical, Erlangen, Germany). Scanning parameters were as follow: repetition time = 1900 ms, echo time = 2.52 ms, flip angle = 9 degrees, inversion time = 900 ms, resolution matrix = 256×256 , slice thickness = 1.0 mm, 176 slices.

Validation dataset 3

T1-weighted anatomical images were scanned on one of two 3 T Siemens Trio scanners, located at the Ahmanson-Lovelace Brain Mapping Center (Siemens version syngo MR B15) and the Staglin Center for Cognitive Neuroscience (Siemens version syngo MR B17) at UCLA. scanning parameters were as follow: repetition time = 1900 ms, echo time = 2.26 ms, field of view = 250 mm, resolution matrix = 256×256 , slice thickness = 1.0 mm, 176 slices.

Individualized gray matter volume variations

Voxel-wise gray matter volume variations (GMV) was determined with voxel based morphometry analysis (VBM) equipped in the Computational Anatomy Toolbox (CAT12, <http://dbm.neuro.uni-jena.de/cat12/>)⁷⁵. We followed the recommended procedures of CAT12 and smoothed the obtained gray matter maps using a 6 mm full width at half maximum Gaussian kernel^{6,77}. The total intracranial volume (TIV) was recorded for the following procedures^{54,78}. For patients in the DIRECT project, we directly smoothed the released gray matter maps obtained using the Data Processing Assistant for Resting-State fMRI (DPARSF) protocol⁷⁹. The cerebellum was not included in the VBM analysis due to incomplete cerebellum scans for some participants.

As previously described, Gaussian process regression was constructed to infer voxel-level GMV from sex and age^{15,17,27}. This model has been proven to perform robustly across different cohorts²⁷. The model trained using HCs was applied to patients with psychiatric disorders to infer the GMV. For each voxel of a given patient, a Z score was calculated to quantify the deviation of the predicted GMV from normal distributions^{15,17,27}. Positive Z scores indicated higher GMV in patients than that of HCs and vice versa.

Modeling ND factors

As previously described²⁷, we parsed individualized gray matter volume variations into potential neuroanatomical differential patterns (ND factors) using NMF^{20,25}. We divided morphological differences into positive and negative parts (henceforth referred to as the positive and negative factors) according to the Z scores. The following analyses were performed separately on the two parts. For the negative part, we used the absolute Z scores. NMF is

defined as follows:

$$D = W \times F + \epsilon, W, F > 0 \quad (1)$$

Where D denotes individualized gray matter volume variations (subject \times voxel); F, neuroanatomical factors (factor \times voxel); W (subject \times the number of factors K), factor compositions (weights); and ϵ , the residuals. The optimal number of factors (K) needed to be predefined.

Based on a previous study²³, we adopted an strategy to automatically determine the optimal K (2–10), assuming that the optimal K yielded the most generalizable factors for unseen patients. Generalizability was measured by increased out-of-sample reconstruction/generalizability error (GE), which was defined as the mean of absolute differences between the reconstructed out-of-sample Z scores using the trained NMF and true ones. A higher GE indicates a worse generalizability. Specifically, for each number of factors, patients were randomly split into two (subsets 1 and 2). The NMF was trained based on subset 1 and applied subset 2. The mean absolute reconstruction error (between the reconstructed and true Z scores) of subset 1 (ϵ_{11}) and 2 (ϵ_{12}) were calculated. Similarly, ϵ_{22} and ϵ_{21} were calculated. GE was calculated using the following formula:

$$GE = \epsilon_{12} - \epsilon_{11} + \epsilon_{21} - \epsilon_{22} \quad (2)$$

This procedure was repeated 100 times. The optimal K value is the number with the lowest average GE value. Most critically, a series of sensitivity analyses were performed to assess the robustness and generalization of the identified ND factors (see Statistics and reproducibility).

Association between ND factors and group-level gray matter volume variations

Group-level gray matter volume variations were obtained using a two-sample t test with SPM12 software (<http://www.fil.ion.ucl.ac.uk/spm/>), where sex, age, and TIV (if any) were included as covariates. The significance of the multilinear models was assessed using one-sided permutation testing (10,000 permutations) and corrected for multiple testing with FDR correction.

To intuitively show the association between individualized and group-level morphological abnormalities, we embedded the factor compositions of each patient and disorder (or all disorders) into a two-dimensional space using t-distributed stochastic neighbor embedding method²⁹. For the group-level morphological abnormalities, the estimated coefficients of the multilinear models were considered as disorder factor compositions.

Association between ND factors and cognitive processes

Functional annotation was performed to associate the identified ND factors with functional terms/cognitive processes. Briefly, functional annotation associates functional terms/cognitive processes with the identified brain regions using probabilistic mappings (<https://neurosynth.org/>)⁸⁰. Probabilistic mappings associate voxels with functional terms (such as mood and autobiographical memory) by synthesizing results from about 15,000 studies⁸⁰. In this study, we only considered 217 terms that bore clear biological significance, according to Cheng et al.⁸¹. Similar to the gene enrichment analysis, function annotation assesses the association between the identified ND factors and certain cognitive processes by determining whether voxels within a cluster have a higher probability of being co-activated by the same functional terms than randomly selected voxels⁸². The significance of this association was assessed using one-sided permutation testing (10,000 times)⁸². Functional terms were considered significant if $p < 0.05$ (uncorrected). For each factor, functional annotation was performed on the top 10% of the voxels with the largest F values using brain annotation toolbox (BAT version 1.1, <https://istbi.fudan.edu.cn/lnen/info/1173/1788.htm>)⁸². Please note, we only considered 217 cognitive terms that did not cover the entire range of human cognitive ontology. Detailed relationships between brain regions and much broader cognitive terms still warrants further research and beyond the scope of this study.

Contribution of neurotransmitter receptors/transporters to ND factors

Therefore, we investigated the contribution of molecular vulnerability to the identified ND factors. To this end, we fitted four multilinear models of neurotransmitter receptors/transporters and each ND factor separately. The significance of the multilinear models was assessed using one-sided permutation testing (10,000 permutations) and corrected for multiple testing with FDR correction. Neurotransmitter receptors/transporters were obtained from PET-derived neurotransmitter receptors/transporters atlas collected and shared by Hansen et al.⁵². The neurotransmitter receptors/transporters include serotonin (5HT_{1A}⁸³, 5HT_{1B}^{83–89}, 5HT_{2A}⁹⁰, 5HT_{2C}⁹⁰, 5HT₆^{91,92}, 5HTT⁹⁰), norepinephrine ($\alpha_1\beta_2$ ^{89,93}, M₁⁹⁴, VACHT^{95,96}), cannabinoid (CB₁^{97–100}), dopamine (D₁¹⁰¹, D₂^{102–105}, DAT¹⁰⁶), GABA (GABA_A¹⁰⁷), histamine (H₃¹⁰⁸), glutamate (mGluR₅^{109,110}, NMDA^{111,112}), opioid (MOR¹¹³), and norepinephrine (NET^{114–117}). For consistency with previous studies^{30,52}, we restricted our analyses to the cortex using processed neurotransmitter receptor/transporter Z scores provided by Hansen et al. (<https://github.com/netneurolab/neuromaps>)⁵².

Thereafter, for each multilinear model, a dominance analysis was performed to further assess the relative importance ('dominance') of predictors (neurotransmitter receptors/transporters) to the overall fit¹¹⁸. Briefly, dominance analysis can be used to estimate the relative importance of predictors by fitting the same multilinear model to all possible combinations of predictors ($2^n - 1$ subset models for a model with n predictors). In this study, total dominance was used to represent the relative importance of the predictors^{30,118}. The total dominance of each predictor is defined as the average of the additional variance (R^2) when added it to the sub-models^{118,119}.

Determining disease epicenters of the ND factors using network diffusion modeling

In healthy population, a structural covariance network was obtained by calculating the pairwise Pearson's correlation coefficients between the mean GMV of each region defined in the Brain Connectome atlas^{120–122}. Age, sex and age² were first regressed from the regional GMV^{33,60,123}. An NDM was built to model the pathological progression on the healthy structural covariance network. The NDM can be modeled as follows:

$$\frac{dx_t}{dt} = -\beta Hx(t) \quad (3)$$

Where $x(t) = x_i(t)$ is the regional pathology (regional values for each ND factor) vector at time t . β is a global diffusivity constant controlling the speed of pathological progression, and its exact value is arbitrary. H is the graph Laplacian $H = I - D^{-\frac{1}{2}}GD^{-\frac{1}{2}}$ where D is a diagonal matrix whose diagonal entries are the weighted degrees of each node.

The regional pathology vector x at time t can be obtained using the equation:

$$x(t) = e^{(-\beta Ht)}x_0 \quad (4)$$

where x_0 denotes the initial pathological distribution at time zero. The unit of time t is arbitrary (a.u.). In this study, β was set to 0.5 such that the peak correlation between NDM-predicted abnormalities and empirical atrophy would occur at 5–10 years^{35,37}. Future studies could estimate the t and β using longitudinal data.

Each region was considered the seed region (disease epicenter), where x_0 was 1 at the seed region and 0 at all other brain regions¹²⁰. Spearman's correlation coefficient (R) between the regional ND factor and NDM-predicted values was calculated for each time point t (between 1 and 50) and region. This procedure would yield 246 (the number of regions) \times 50 correlation matrices (referred to as 'R-t curves'). The maximum value of R (mR) was recorded for each region. The brain region with the maximum mR was considered the putative seed region.

Subtyping patients based on factor compositions

Finally, we investigated whether factor composition could help reveal the transdiagnostic subtypes. The K-means algorithm was used to identify the transdiagnostic subtypes, with factor compositions as features and the squared Euclidean distance as the distance metric. The optimal number of subtypes ranging from 2 to 10 was determined using silhouette values¹²⁴. For each subtype number, k-means was repeated 100 times to avoid local minima during the initialization of centroid positions¹²⁵.

Statistics and reproducibility

Robustness and Reproducibility analysis of the identified ND factors. A series of sensitivity analyses were performed to assess the robustness and generalization of the identified ND factors. First, internal validation was performed using 10-fold cross-validation. For each run, we trained the NMF based on the training set and used the trained NMF to predict the factor compositions (W) of the patients in the testing set. Pearson's correlation coefficients between the true factor compositions obtained using all patients, and the predicted ones across runs were calculated. This procedure was performed 100 times to minimize random selection errors. Second, leave-one-disorder-out cross-validation was performed. We trained the NMF based on patients with two disorders (such as depression and OCD) and predicted the factor compositions of patients with the remaining disorder (such as schizophrenia). Third, we calculated spatial correlations between the ND factors obtained using different datasets. The correspondence between ND factors obtained using different datasets was determined using the Hungarian matching algorithm^{24,126}. The correlations significance was assessed using one-sided permutation testing (10,000 permutations) and corrected for multiple testing using Benjamini-Hochberg false discovery rate (FDR) correction. Forth, we predicted factor compositions of patients in validation datasets based on the NMF trained using the discovery dataset. Pearson's correlation coefficients between the predicted and the true factor compositions were calculated. The significance of the correlations was corrected for multiple testing using FDR correction.

Significance of NDM. NDM significance was assessed by constructing 10,000 random networks¹²⁷. For each random network, we rerun the NDM and recorded the maximum Spearman's correlation coefficient (R_{rand}) across time and brain regions. This procedure yielded a null distribution to assess the significance of the NDM based on the true network.

Robustness and reproducibility analysis of clustering results. Two strategies were used to assess the stability of the clustering results. First, we randomly selected 90% of patients and performed k-means clustering on this subsample (repeating 100 times). ARI between the subtyping results obtained using the subsample and those obtained using all patients was calculated. Second, we used a completely different clustering algorithm, called heterogeneity through discriminative analysis (HYDRA) with regional GMV as features¹²⁸. As a semi-supervised method, the HYDRA succeeds in uncovering distinct subtypes in psychiatric disorders^{39,66,129}. The HYDRA automatically determines the optimal number of clusters based on the adjusted Rand index (ARI), quantifying the similarity between the clustering results of cross-validation¹²⁸. The optimal number of clusters was determined when the ARI was the largest. In this study, we determined the optimal subtypes from 2 to 10 using 10-fold cross-validation, controlling for age and sex. The Adjusted Rand Index (ARI) between HYDRA subtyping results and those reported previously was calculated.

Statistical analyses in morphological and clinical differences between the subtypes. We examined the morphological and clinical differences between the subtypes. Specifically, we obtained voxel-wise morphological differences in each subtype or in all patients compared with HCs using a two-sample t test with SPM12, controlling for sex, age,

and TIV (any). The significance was set at Bonferroni-corrected $p < 0.05$. We then investigated whether the clinical features differed between the subtypes, including age, sex, symptom severity, illness duration, and age of onset for each diagnosis.

Reporting summary

Further information on research design is available in the Nature Portfolio Reporting Summary linked to this article.

Data availability

The probabilistic mappings are provided by Neurosynth (<https://neurosynth.org/>). The discovery dataset is available from the corresponding author upon request. The validation datasets are freely available (Validation dataset 1: http://fcon_1000.projects.nitrc.org/indi/retro/cobre.html; Validation dataset 2: <https://www.scidb.cn/en/detail?datasetId=cbeb3c7124bf47a6af7b3236a3aaf3a8>; Validation dataset 3: <https://openneuro.org/datasets/ds000030/versions/00016>). PET images are available at <https://github.com/netneurolab/neuromaps>.

Code availability

All analytical procedures are based on publicly available toolkits. Voxel-wise gray matter volume is obtained using the Computational Anatomy Toolbox (CAT12, <http://dbm.neuro.uni-jena.de/cat12/>)¹³⁰. The normative modeling is constructed using GAUSSIAN PROCESS REGRESSION AND CLASSIFICATION Toolbox 4.2 (<http://www.GaussianProcess.org/gpml/code>)¹³¹. The Brain Annotation Toolbox (version 1.1) is available at <https://istbi.fudan.edu.cn/lneen/info/1173/1788.htm>⁸². Group-level gray matter volume differences are obtained using SPM12 (<http://www.fil.ion.ucl.ac.uk/spm>)¹³². Non-negative matrix factorization is performed using scikit-learn 1.3.2 (<https://scikit-learn.org/stable/>)^{133,134}.

Received: 22 July 2024; Accepted: 7 February 2025;

Published online: 14 February 2025

References

- Barch, D. M. & Sheffield, J. M. Cognitive impairments in psychotic disorders: common mechanisms and measurement. *World Psychiatry* **13**, 224–232 (2014).
- Sonuga-Barke, E. Identification of risk loci with shared effects on five major psychiatric disorders: a genome-wide analysis. *Lancet* **381**, 1371–1379 (2013).
- Anttila, V. et al. Analysis of shared heritability in common disorders of the brain. *Science* **360**, eaap8757 (2018).
- Caspi, A. et al. The p Factor: One General Psychopathology Factor in the Structure of Psychiatric Disorders? *Clin. Psychological Sci.* **2**, 119–137 (2014).
- Identification of risk loci with shared effects on five major psychiatric disorders: a genome-wide analysis. *The Lancet* **381**, 1371–1379 (2013).
- Menon, V. Large-scale brain networks and psychopathology: a unifying triple network model. *Trends Cogn. Sci.* **15**, 483–506 (2011).
- Whitfield-Gabrieli, S. & Ford, J. M. Default Mode Network Activity and Connectivity in Psychopathology. *Annu. Rev. Clin. Psychol.* **8**, 49–76 (2012).
- Segal, A. et al. Regional, circuit and network heterogeneity of brain abnormalities in psychiatric disorders. *Nat. Neurosci.* **26**, 1613–1629 (2023).
- Amone, D., McIntosh, A. M., Ebmeier, K. P., Munafò, M. R. & Anderson, I. M. Magnetic resonance imaging studies in unipolar depression: Systematic review and meta-regression analyses. *Eur. Neuropsychopharmacol.* **22**, 1–16 (2012).
- Goodkind, M. et al. Identification of a Common Neurobiological Substrate for Mental Illness. *JAMA Psychiatry* **72**, 305–315 (2015).
- Bondar, J., Caye, A., Chekroud, A. M. & Kieling, C. Symptom clusters in adolescent depression and differential response to treatment: a secondary analysis of the Treatment for Adolescents with Depression Study randomised trial. *Lancet Psychiatry* **7**, 337–343 (2020).
- Krishnan, V. & Nestler, E. J. The molecular neurobiology of depression. *Nature* **455**, 894–902 (2008).
- Drysdale, A. T., Grosenick, L. & Downar, J. Resting-state connectivity biomarkers define neurophysiological subtypes of depression. *Nat. Med.* **23**, 28–38 (2017).
- Nguyen, T. D., Harder, A., Xiong, Y., Kowalec, K. & Hägg, S. Genetic heterogeneity and subtypes of major depression. *Mol. Psychiatry* **27**, 1667–1675 (2022).
- Wolfers, T. et al. Mapping the Heterogeneous Phenotype of Schizophrenia and Bipolar Disorder Using Normative Models. *JAMA Psychiatry* **75**, 1146–1155 (2018).
- Chen, Z. et al. High-field magnetic resonance imaging of structural alterations in first-episode, drug-naïve patients with major depressive disorder. *Transl. Psychiatry* **6**, e942 (2016).
- Marquand, A. F., Rezek, I., Buitelaar, J. & Beckmann, C. F. Understanding Heterogeneity in Clinical Cohorts Using Normative Models: Beyond Case-Control Studies. *Biol. Psychiatry* **80**, 552–561 (2016).
- Wolfers, T. & Beckmann, C. F. Individual differences v. the average patient: mapping the heterogeneity in ADHD using normative models. *Psychol. Med.* **50**, 314–323 (2020).
- Zabihi, M. et al. Dissecting the Heterogeneous Cortical Anatomy of Autism Spectrum Disorder Using Normative Models. *Biol. Psychiatry Cogn. Neurosci. Neuroimaging* **4**, 567–578 (2019).
- Shan, X. et al. Mapping the Heterogeneous Brain Structural Phenotype of Autism Spectrum Disorder Using the Normative Model. *Biol. Psychiatry* **91**, 967–976 (2022).
- Shao, J. N. et al. Capturing the Individual Deviations From Normative Models of Brain Structure for Depression Diagnosis and Treatment. *Biol. Psychiatry* **95**, 403–413 (2023).
- Tong, X. et al. Individual deviations from normative electroencephalographic connectivity predict antidepressant response. *J. Affect Disord.* **351**, 220–230 (2024).
- Chen, J. et al. Neurobiological Divergence of the Positive and Negative Schizophrenia Subtypes Identified on a New Factor Structure of Psychopathology Using Non-negative Factorization: An International Machine Learning Study. *Biol. Psychiatry* **87**, 282–293 (2020).
- Zhang, X. et al. Bayesian model reveals latent atrophy factors with dissociable cognitive trajectories in Alzheimer's disease. *Proc. Natl. Acad. Sci. USA* **113**, E6535–e6544 (2016).
- Anderson, A. et al. Non-negative matrix factorization of multimodal MRI, fMRI and phenotypic data reveals differential changes in default mode subnetworks in ADHD. *NeuroImage* **102**, 207–219 (2014).
- Sotiras, A. et al. Patterns of coordinated cortical remodeling during adolescence and their associations with functional specialization and evolutionary expansion. *Proc. Natl. Acad. Sci. USA* **114**, 3527–3532 (2017).
- Han, S. et al. Parsing altered gray matter morphology of depression using a framework integrating the normative model and non-negative matrix factorization. *Nat. Commun.* **14**, 4053 (2023).
- Yeo, B. T. et al. The organization of the human cerebral cortex estimated by intrinsic functional connectivity. *J. Neurophysiol.* **106**, 1125–1165 (2011).
- Laurens, V. D. M. & Hinton, G. Visualizing Data using t-SNE. *J. Mach. Learn. Res.* **9**, 2579–2605 (2008).
- Hansen, J. Y. & Shafiei, G. Local molecular and global connectomic contributions to cross-disorder cortical abnormalities. *Nat. Commun.* **13**, 4682 (2022).
- Zhou, J., Gennatas, E. D., Kramer, J. H., Miller, B. L. & Seeley, W. W. Predicting regional neurodegeneration from the healthy brain functional connectome. *Neuron* **73**, 1216–1227 (2012).

32. Yau, Y., Zeighami, Y., Baker, T. E., Larcher, K. & Vainik, U. Network connectivity determines cortical thinning in early Parkinson's disease progression. *Nat. Commun.* **9**, 12 (2018).
33. Wannan, C. M. J. et al. Evidence for Network-Based Cortical Thickness Reductions in Schizophrenia. *Am. J. Psychiatry* **176**, 552–563 (2019).
34. Shafiei, G. et al. Spatial Patterning of Tissue Volume Loss in Schizophrenia Reflects Brain Network Architecture. *Biol. Psychiatry* **87**, 727–735 (2020).
35. Raj, A., Kuceyeski, A. & Weiner, M. A network diffusion model of disease progression in dementia. *Neuron* **73**, 1204–1215 (2012).
36. Raj, A. et al. Network Diffusion Model of Progression Predicts Longitudinal Patterns of Atrophy and Metabolism in Alzheimer's Disease. *Cell Rep.* **10**, 359–369 (2015).
37. Pandya, S. et al. Predictive model of spread of Parkinson's pathology using network diffusion. *NeuroImage* **192**, 178–194 (2019).
38. Hooker, C. I., Bruce, L., Lincoln, S. H., Fisher, M. & Vinogradov, S. Theory of mind skills are related to gray matter volume in the ventromedial prefrontal cortex in schizophrenia. *Biol. Psychiatry* **70**, 1169–1178 (2011).
39. Chand, G. B. et al. Two distinct neuroanatomical subtypes of schizophrenia revealed using machine learning. *Brain J. Neurol.* **143**, 1027–1038 (2020).
40. Yu, M. et al. Childhood trauma history is linked to abnormal brain connectivity in major depression. *Proc. Natl. Acad. Sci. USA* **116**, 8582–8590 (2019).
41. Boedhoe, P. S. W. et al. Cortical Abnormalities Associated With Pediatric and Adult Obsessive-Compulsive Disorder: Findings From the ENIGMA Obsessive-Compulsive Disorder Working Group. *Am. J. Psychiatry* **175**, 453–462 (2018).
42. Rodriguez-Murillo, L., Gogos, J. A. & Karayiorgou, M. The genetic architecture of schizophrenia: new mutations and emerging paradigms. *Annu. Rev. Med.* **63**, 63–80 (2012).
43. Dong, D. B., et al. Functional Connectome Hierarchy in Schizotypy and Its Associations With Expression of Schizophrenia-Related Genes. *Schizophrenia Bull.* **51**, 145–158 (2023).
44. Xia, M. et al. Shared and Distinct Functional Architectures of Brain Networks Across Psychiatric Disorders. *Schizophrenia Bull.* **45**, 450–463 (2019).
45. Chang, M. et al. Neurobiological Commonalities and Distinctions Among Three Major Psychiatric Diagnostic Categories: A Structural MRI Study. *Schizophrenia Bull.* **44**, 65–74 (2018).
46. Hettwer, M. D., Larivière, S. & Park, B. Y. Coordinated cortical thickness alterations across six neurodevelopmental and psychiatric disorders. *Nat. Commun.* **13**, 6851 (2022).
47. Opel, N. et al. Cross-Disorder Analysis of Brain Structural Abnormalities in Six Major Psychiatric Disorders: A Secondary Analysis of Mega- and Meta-analytical Findings From the ENIGMA Consortium. *Biol. Psychiatry* **88**, 678–686 (2020).
48. Radonjić, N. V. & Hess, J. L. Structural brain imaging studies offer clues about the effects of the shared genetic etiology among neuropsychiatric disorders. *Mol. Psychiatry* **26**, 2101–2110 (2021).
49. Sun, X. et al. Mapping Neurophysiological Subtypes of Major Depressive Disorder Using Normative Models of the Functional Connectome. *Biol. Psychiatry* **94**, 936–947 (2023).
50. Han, S. Q. et al. Mapping the neuroanatomical heterogeneity of OCD using a framework integrating normative model and non-negative matrix factorization. *Cereb. Cortex* **33**, 8667–8678 (2023).
51. Elad, D. et al. Improving the predictive potential of diffusion MRI in schizophrenia using normative models-Towards subject-level classification. *Hum. Brain Mapp.* **42**, 4658–4670 (2021).
52. Hansen, J. Y. & Shafiei, G. Mapping neurotransmitter systems to the structural and functional organization of the human neocortex. *Nat. Neurosci.* **25**, 1569–1581 (2022).
53. Warren, J. D. et al. Molecular nexopathies: a new paradigm of neurodegenerative disease. *Trends Neurosci.* **36**, 561–569 (2013).
54. Brown, J. A. et al. Patient-Tailored, Connectivity-Based Forecasts of Spreading Brain Atrophy. *Neuron* **104**, 856–868.e855 (2019).
55. Zeighami, Y., et al. Network structure of brain atrophy in de novo Parkinson's disease. *Elife* **4**, e08440 (2015).
56. Dong, D. et al. Reconfiguration of Dynamic Functional Connectivity in Sensory and Perceptual System in Schizophrenia. *Cereb. Cortex* **29**, 3577–3589 (2019).
57. Butler, P. D. et al. Sensory contributions to impaired emotion processing in schizophrenia. *Schizophrenia Bull.* **35**, 1095–1107 (2009).
58. Fang, Q. et al. Transcriptional substrates of brain structural and functional impairments in drug-naïve first-episode patients with major depressive disorder. *J. Affect. Disord.* **325**, 522–533 (2023).
59. Dong, D. et al. Linking cerebellar functional gradients to transdiagnostic behavioral dimensions of psychopathology. *NeuroImage Clin.* **36**, 103176 (2022).
60. Wang, Y. L., et al. Volume of the Dentate Gyrus/CA4 Hippocampal subfield mediates the interplay between sleep quality and depressive symptoms. *Int. J. Clin. Health Psychol.* **24**, 100432 (2024).
61. Beijers, L., Wardenaar, K. J., van Loo, H. M. & Schoevers, R. A. Data-driven biological subtypes of depression: systematic review of biological approaches to depression subtyping. *Mol. Psychiatry* **24**, 888–900 (2019).
62. Mataix-Cols, D. et al. Distinct neural correlates of washing, checking, and hoarding symptom dimensions in obsessive-compulsive disorder. *Arch. Gen. Psychiatry* **61**, 564–576 (2004).
63. Lynch, C. J., Gunning, F. M. & Liston, C. Causes and Consequences of Diagnostic Heterogeneity in Depression: Paths to Discovering Novel Biological Depression Subtypes. *Biol. Psychiatry* **88**, 83–94 (2020).
64. Derks, E. M. et al. Kraepelin was right: a latent class analysis of symptom dimensions in patients and controls. *Schizophrenia Bull.* **38**, 495–505 (2012).
65. Han, S. et al. Resolving heterogeneity in depression using individualized structural covariance network analysis. *Psychological Med.* **53**, 5312–5321 (2023).
66. Han, S., Xu, Y., Guo, H. R., Fang, K. & Wei, Y. Two distinct subtypes of obsessive compulsive disorder revealed by heterogeneity through discriminative analysis. *Hum. Brain Mapp.* **43**, 3037–3046 (2022).
67. Collin, G., Kahn, R. S., de Reus, M. A., Cahn, W. & van den Heuvel, M. P. Impaired rich club connectivity in unaffected siblings of schizophrenia patients. *Schizophrenia Bull.* **40**, 438–448 (2014).
68. Yan, C. G. et al. Reduced default mode network functional connectivity in patients with recurrent major depressive disorder. *Proc. Natl. Acad. Sci. USA* **116**, 9078–9083 (2019).
69. Chen, X. et al. The DIRECT consortium and the REST-meta-MDD project: towards neuroimaging biomarkers of major depressive disorder. *Psychoradiology* **2**, 32–42 (2022).
70. Poldrack, R. A. et al. A phenome-wide examination of neural and cognitive function. *Sci. Data* **3**, 160110 (2016).
71. Hamilton, M. A rating scale for depression. *J. Neurol. Neurosurg. Psychiatry* **23**, 56–62 (1960).
72. Kay, S. R., Fiszbein, A. & Opler, L. A. The positive and negative syndrome scale (PANSS) for schizophrenia. *Schizophrenia Bull.* **13**, 261–276 (1987).
73. Goodman, W. K. et al. The Yale-Brown Obsessive Compulsive Scale. I. Development, use, and reliability. *Arch. Gen. Psychiatry* **46**, 1006–1011 (1989).
74. Kebets, V. et al. Somatosensory-Motor Dysconnectivity Spans Multiple Transdiagnostic Dimensions of Psychopathology. *Biol. Psychiatry* **86**, 779–791 (2019).

75. Ashburner, J. & Friston, K. J. Voxel-based morphometry-the methods. *NeuroImage* **11**, 805–821 (2000).
76. Ashburner, J. Computational anatomy with the SPM software. *Magn. Reson. imaging* **27**, 1163–1174 (2009).
77. Han, S., et al. Progressive brain structural abnormality in depression assessed with MR imaging by using causal network analysis. *Psychological Med.*, **53**, 2146–2155 (2021).
78. Han, S., et al. Resolving heterogeneity in obsessive-compulsive disorder through individualized differential structural covariance network analysis. *Cerebral Cortex* **33**, 1659–1668 (2022).
79. Chao-Gan, Y. & Yu-Feng, Z. DPARSF: A MATLAB Toolbox for “Pipeline” Data Analysis of Resting-State fMRI. *Front. Syst. Neurosci.* **4**, 13 (2010).
80. Yarkoni, T., Poldrack, R. A., Nichols, T. E., Van Essen, D. C. & Wager, T. D. Large-scale automated synthesis of human functional neuroimaging data. *Nat. Methods* **8**, 665–670 (2011).
81. Cheng, W. et al. Functional connectivity decreases in autism in emotion, self, and face circuits identified by Knowledge-based Enrichment Analysis. *NeuroImage* **148**, 169–178 (2017).
82. Liu, Z. et al. Brain annotation toolbox: exploring the functional and genetic associations of neuroimaging results. *Bioinforma* **35**, 3771–3778 (2019).
83. Savli, M. et al. Normative database of the serotonergic system in healthy subjects using multi-tracer PET. *NeuroImage* **63**, 447–459 (2012).
84. Gallezot, J. D. et al. Kinetic modeling of the serotonin 5-HT(1B) receptor radioligand [(11C)P943] in humans. *J. Cereb. Blood Flow. Metab.* **30**, 196–210 (2010).
85. Murrough, J. W. et al. The effect of early trauma exposure on serotonin type 1B receptor expression revealed by reduced selective radioligand binding. *Arch. Gen. Psychiatry* **68**, 892–900 (2011).
86. Murrough, J. W. et al. Reduced ventral striatal/ventral pallidal serotonin1B receptor binding potential in major depressive disorder. *Psychopharmacology* **213**, 547–553 (2011).
87. Matuskey, D. et al. Reductions in brain 5-HT1B receptor availability in primarily cocaine-dependent humans. *Biol. Psychiatry* **76**, 816–822 (2014).
88. Saricicek, A. et al. Test-retest reliability of the novel 5-HT1B receptor PET radioligand [11C]P943. *Eur. J. Nucl. Med. Mol. Imaging* **42**, 468–477 (2015).
89. Baldassarri, S. R. et al. Use of Electronic Cigarettes Leads to Significant Beta2-Nicotinic Acetylcholine Receptor Occupancy: Evidence From a PET Imaging Study. *Nicotine Tob. Res.* **20**, 425–433 (2018).
90. Beliveau, V. & Ganz, M. A High-Resolution In Vivo Atlas of the Human Brain's. *Serotonin Syst.* **37**, 120–128 (2017).
91. Radhakrishnan, R. et al. Age-Related Change in 5-HT(6) Receptor Availability in Healthy Male Volunteers Measured with (11)C-GSK215083 PET. *J. Nucl. Med.* **59**, 1445–1450 (2018).
92. Radhakrishnan, R. et al. In vivo 5-HT(6) and 5-HT(2A) receptor availability in antipsychotic treated schizophrenia patients vs. unmedicated healthy humans measured with [(11)C]GSK215083 PET. *Psychiatry Res. Neuroimaging* **295**, 111007 (2020).
93. Hillmer, A. T. et al. Imaging of cerebral $\alpha 4\beta 2^*$ nicotinic acetylcholine receptors with (-)-[(18)F]Flubatine PET: Implementation of bolus plus constant infusion and sensitivity to acetylcholine in human brain. *NeuroImage* **141**, 71–80 (2016).
94. Naganawa, M. et al. First-in-Human Assessment of (11)C-LSN3172176, an M1 Muscarinic Acetylcholine Receptor PET Radiotracer. *J. Nucl. Med.* **62**, 553–560 (2021).
95. Aghourian, M., Legault-Denis, C., Soucy, J. P., Rosa-Neto, P. Quantification of brain cholinergic denervation in Alzheimer's disease using PET imaging with [(18)F]-FEOBV. *Mol. Psychiatry* **22**, 1531–1538 (2017).
96. Bedard, M. A. et al. Brain cholinergic alterations in idiopathic REM sleep behaviour disorder: a PET imaging study with (18)F-FEOBV. *Sleep. Med.* **58**, 35–41 (2019).
97. Normandin, M. D. et al. Imaging the cannabinoid CB1 receptor in humans with [11C]OMAR: assessment of kinetic analysis methods, test-retest reproducibility, and gender differences. *J. Cereb. Blood Flow. Metab.* **35**, 1313–1322 (2015).
98. D'Souza, D. C. et al. Rapid Changes in CB1 Receptor Availability in Cannabis Dependent Males after Abstinence from Cannabis. *Biol. Psychiatry Cogn. Neurosci. Neuroimaging* **1**, 60–67 (2016).
99. Ranganathan, M. et al. Reduced Brain Cannabinoid Receptor Availability in Schizophrenia. *Biol. Psychiatry* **79**, 997–1005 (2016).
100. Neumeister, A. et al. Positron emission tomography shows elevated cannabinoid CB1 receptor binding in men with alcohol dependence. *Alcohol. Clin. Exp. Res.* **36**, 2104–2109 (2012).
101. Kaller, S. et al. Test-retest measurements of dopamine D(1)-type receptors using simultaneous PET/MRI imaging. *Eur. J. Nucl. Med. Mol. Imaging* **44**, 1025–1032 (2017).
102. Smith, C. T. et al. Partial-volume correction increases estimated dopamine D2-like receptor binding potential and reduces adult age differences. *J. Cereb. Blood Flow. Metab.* **39**, 822–833 (2019).
103. Sandiego, C. M. et al. Reference region modeling approaches for amphetamine challenge studies with [11C]FLB 457 and PET. *J. Cereb. Blood Flow. Metab.* **35**, 623–629 (2015).
104. Zakariaeiz, Y. et al. Sex differences in amphetamine-induced dopamine release in the dorsolateral prefrontal cortex of tobacco smokers. *Neuropsychopharmacology* **44**, 2205–2211 (2019).
105. Slifstein, M. et al. Deficits in prefrontal cortical and extrastriatal dopamine release in schizophrenia: a positron emission tomographic functional magnetic resonance imaging study. *JAMA Psychiatry* **72**, 316–324 (2015).
106. Dukart, J. et al. Cerebral blood flow predicts differential neurotransmitter activity. *Sci. Rep.* **8**, 4074 (2018).
107. Nørgaard, M. et al. A high-resolution in vivo atlas of the human brain's benzodiazepine binding site of GABA(A) receptors. *NeuroImage* **232**, 117878 (2021).
108. Gallezot, J. D. et al. Determination of receptor occupancy in the presence of mass dose: [(11)C]GSK189254 PET imaging of histamine H(3) receptor occupancy by PF-03654746. *J. Cereb. Blood Flow. Metab.* **37**, 1095–1107 (2017).
109. Smart, K. et al. Sex differences in [(11)C]ABP688 binding: a positron emission tomography study of mGlu5 receptors. *Eur. J. Nucl. Med. Mol. imaging* **46**, 1179–1183 (2019).
110. DuBois, J. M. et al. Characterization of age/sex and the regional distribution of mGluR5 availability in the healthy human brain measured by high-resolution [(11)C]ABP688 PET. *Eur. J. Nucl. Med. Mol. imaging* **43**, 152–162 (2016).
111. Galovic, M. et al. Validation of a combined image derived input function and venous sampling approach for the quantification of [(18)F]GE-179 PET binding in the brain. *NeuroImage* **237**, 118194 (2021).
112. McGinnity, C. J. et al. Initial evaluation of 18F-GE-179, a putative PET Tracer for activated N-methyl D-aspartate receptors. *J. Nucl. Med.* **55**, 423–430 (2014).
113. Kantonen, T. et al. Interindividual variability and lateralization of μ -opioid receptors in the human brain. *NeuroImage* **217**, 116922 (2020).
114. Ding, Y. S. et al. PET imaging of the effects of age and cocaine on the norepinephrine transporter in the human brain using (S,S)-[(11)C]O-methylreboxetine and HRRT. *Synapse* **64**, 30–38 (2010).
115. Li, C. S. et al. Decreased norepinephrine transporter availability in obesity: Positron Emission Tomography imaging with (S,S)-[(11)C] O-methylreboxetine. *NeuroImage* **86**, 306–310 (2014).
116. Sanchez-Rangel, E. et al. Norepinephrine transporter availability in brown fat is reduced in obesity: a human PET study with [(11)C]MRB. *Int. J. Obes.* **44**, 964–967 (2020).

117. Belfort-DeAguiar, R. et al. Noradrenergic Activity in the Human Brain: A Mechanism Supporting the Defense Against Hypoglycemia. *J. Clin. Endocrinol. Metab.* **103**, 2244–2252 (2018).
 118. Budescu, David V. Dominance analysis : a new approach to the problem of relative importance of predictors in multiple regression. *Psychological Bull.* **114**, 542–551 (1993).
 119. Azen, R. & Budescu, D. V. The dominance analysis approach for comparing predictors in multiple regression. *Psychological methods* **8**, 129–148 (2003).
 120. Fan, L. et al. The Human Brainnetome Atlas: A New Brain Atlas Based on Connectional Architecture. *Cereb. Cortex* **26**, 3508–3526 (2016).
 121. Wang Y. L., et al. Covariance patterns between sleep health domains and distributed intrinsic functional connectivity. *Nat. Commun.* **14**, 7133 (2023).
 122. Wang, Y. L. et al. Altered morphometric similarity networks in insomnia disorder. *Brain Struct. Funct.* **229**, 1433–1445 (2024).
 123. Wang, Y. et al. Individualized morphometric similarity predicts body mass index and food approach behavior in school-age children. *Cereb. Cortex* **33**, 4794–4805 (2023).
 124. Han S., et al. Resolving heterogeneity in depression using individualized structural covariance network analysis. *Psychological Med.* **53**, 5312–5321 (2023).
 125. Allen, E. A. et al. Tracking whole-brain connectivity dynamics in the resting state. *Cereb. Cortex* **24**, 663–676 (2014).
 126. Lee, H. M. et al. Decomposing MRI phenotypic heterogeneity in epilepsy: a step towards personalized classification. *Brain* **145**, 897–908 (2022).
 127. Rubinov, M. & Sporns, O. Weight-conserving characterization of complex functional brain networks. *NeuroImage* **56**, 2068–2079 (2011).
 128. Varol, E., Sotiras, A. & Davatzikos, C. HYDRA: Revealing heterogeneity of imaging and genetic patterns through a multiple max-margin discriminative analysis framework. *NeuroImage* **145**, 346–364 (2017).
 129. Han, S. et al. Progressive brain structural abnormality in depression assessed with MR imaging by using causal network analysis. *Psychological Med.* **53**, 2146–2155 (2023).
 130. Gaser C., Dahnke R., Thompson P. M., Kurth F., Luders E., The Alzheimer's Disease Neuroimaging I. CAT: a computational anatomy toolbox for the analysis of structural MRI data. *GigaScience* **13**, giae049 (2024).
 131. Rasmussen, C. E. & Nickisch, H. Gaussian Processes for Machine Learning (GPML) Toolbox[J]. *Journal of Machine Learning Research* **11**, 3011–3015 (2010).
 132. Ashburner, J. & Friston, K. J. Unified segmentation. *NeuroImage* **26**, 839–851 (2005).
 133. Cichocki A., Phan A. H. J. I. T. F. Fast Local Algorithms for Large Scale Nonnegative Matrix and Tensor Factorizations. In: *IEICE Transactions on Fundamentals of Electronics Communications and Computer Sciences*, 92, 708–721 (IEICE, 2009).
 134. Févotte C., Idier J. Algorithms for nonnegative matrix factorization with the beta-divergence. *Neural Comput.* **23**, 2421 - 2456 (2010).
- project of Henan province (S20240045, SBGJ202302068), the Key Technologies Research and Development Program of Henan Province (222102210076), the Key Scientific Research Program of the Higher Education Institutions of Henan Province (22A416013) and Medical science and technology research project of Henan province (LHGJ20230217).

Author contributions

Shaoqiang Han, Yong Zhang, Jingliang Cheng and Huaifu Chen conceived the study. Shaoqiang Han and Ya Tian Wrote the manuscripts. Ya Tian, Ruiping Zheng, Qiuying Tao, Xueqin Song, Hui-Rong Guo, Baohong Wen, Kangkang Xue, Yuan Chen and Jinming Xiao assisted in patient recruitment. Ya Tian, Ruiping Zheng, Qiuying Tao, Xueqin Song, Hui-Rong Guo, Baohong Wen, Kangkang Xue, Yuan Chen and Liang Liu collected the data. Shaoqiang Han, Jinming Xiao, Yajing Pang and Yarui Wei analyzed the data. All authors contributed to the drafting of the manuscripts and approved the submitted version.

Competing interests

The authors declare no competing interests.

Additional information

Supplementary information The online version contains supplementary material available at <https://doi.org/10.1038/s42003-025-07703-x>.

Correspondence and requests for materials should be addressed to Shaoqiang Han, Kangkang Xue, Yuan Chen, Jingliang Cheng or Yong Zhang.

Peer review information *Communications Biology* thanks Donato Liloia, Thomas Nickl-Jockschat, and Manuel Martín-Loeches for their contribution to the peer review of this work. Primary Handling Editors: Marta Vallejo and Jasmine Pan.

Reprints and permissions information is available at <http://www.nature.com/reprints>

Publisher's note Springer Nature remains neutral with regard to jurisdictional claims in published maps and institutional affiliations.

Open Access This article is licensed under a Creative Commons Attribution-NonCommercial-NoDerivatives 4.0 International License, which permits any non-commercial use, sharing, distribution and reproduction in any medium or format, as long as you give appropriate credit to the original author(s) and the source, provide a link to the Creative Commons licence, and indicate if you modified the licensed material. You do not have permission under this licence to share adapted material derived from this article or parts of it. The images or other third party material in this article are included in the article's Creative Commons licence, unless indicated otherwise in a credit line to the material. If material is not included in the article's Creative Commons licence and your intended use is not permitted by statutory regulation or exceeds the permitted use, you will need to obtain permission directly from the copyright holder. To view a copy of this licence, visit <http://creativecommons.org/licenses/by-nc-nd/4.0/>.

© The Author(s) 2025

Acknowledgements

This research study was supported by the Natural Science Foundation of China (62476252, 82471962), Medical science and technology research